



HAL
open science

Deposition and patterning of electrodes on the vertical sidewalls of deep trenches

Lucas Bonnin, Adrien Piot, Nathalie Isac, Alain Bosseboeuf

► **To cite this version:**

Lucas Bonnin, Adrien Piot, Nathalie Isac, Alain Bosseboeuf. Deposition and patterning of electrodes on the vertical sidewalls of deep trenches. *Journal of Micromechanics and Microengineering*, 2020, 30 (10), pp.105014. 10.1088/1361-6439/aba377 . hal-03029383

HAL Id: hal-03029383


<https://hal.science/hal-03029383>

Submitted on 23 Dec 2020

HAL is a multi-disciplinary open access archive for the deposit and dissemination of scientific research documents, whether they are published or not. The documents may come from teaching and research institutions in France or abroad, or from public or private research centers.

L'archive ouverte pluridisciplinaire **HAL**, est destinée au dépôt et à la diffusion de documents scientifiques de niveau recherche, publiés ou non, émanant des établissements d'enseignement et de recherche français ou étrangers, des laboratoires publics ou privés.

Deposition and patterning of electrodes on the vertical sidewalls of deep trenches

L. Bonnin^{1,2} , A. Piot^{1,2,3}, N. Isac¹, A. Bosseboeuf¹

¹ C2N, CNRS, University Paris Saclay, 10 Bd Thomas Gobert, 91120 Palaiseau, France

² ONERA - The French Aerospace Lab, 29 Avenue de la division Leclerc, 92320 Chatillon, France

³ Silicon Austria Labs GmbH, High Tech campus Villach-Europastraße 12, A-9524, Villach, Austria

E-mail: alain.bosseboeuf@c2n.upsaclay.fr

Received xxxxxx

Accepted for publication xxxxxx

Published xxxxxx

Abstract

A process able to produce at wafer scale patterned electrodes on the vertical sidewalls of trenches is described and investigated in details. It is based on metal evaporation at oblique incidence through a shadow mask made in a dry photoresist film. A full model of the deposition and patterning process is established in order to map the shape as well as the thickness and density of patterned electrodes with or without wafer rotation. In the case of wafer rotation, the modelling is based on the analogy of each shadow mask edge with the gnomon of a sundial. The final electrode shape is then computed from the trajectories followed by the shadows of the gnomons. Offset of the substrate tilt axis with respect to substrate plane, and position on the wafer surface, are considered in the analysis, as well as the variation of film density with incidence angle. Advantages and limitations of the proposed process are discussed. It is shown that sidewalls electrodes isolated or connected to top or bottom electrodes can be simply achieved by a suitable sizing and alignment of the shadow mask but that close electrodes on a given sidewall cannot be mutually isolated when the substrate is rotated. The patterning process is demonstrated in the case of Au/Cr electrodes on the sidewalls of through wafer trenches made in GaAs by deep reactive ion etching.

Keywords: evaporation, patterning, vertical sidewalls, shadow masking, gnomonics

1. Introduction

The ability to pattern films on vertical or highly tilted sidewalls of etched 3D microstructures can be greatly beneficial for many kinds of devices and advanced packaging technologies [1-10]. In the last ten years, various processes were proposed to pattern bare or coated surfaces on the sidewalls of trenches or microstructures with vertical sidewalls. Recently, a process based on conformal deposition of three LPCVD masking layers (SiO_2 , SiN_x and Poly Si), on selective chemical etchings steps and on tilted ion milling was used to remove the top part, middle part or bottom part of an underlying SiO_2 layer deposited on the sidewalls of

microstructures like pillars [1]. This SiO_2 patterning technique was used as a mask for electroplating Ni-Mo layers on Si microwires to fabricate photocathodes [2]. This process can be applied at wafer scale to high aspect ratio microstructures of any shape with apertures around them having an aspect ratio up to 5 or more. It has a high patterning resolution but requires a large number of deposition and etching steps. In the case of a photosensitive glass structure, sidewalls electrodes could be patterned by water assisted femto laser spatial etching followed by Au/Cr electroless plating [3]. For patterning films with an aspect ratio close or lower than 1, simpler processes based on

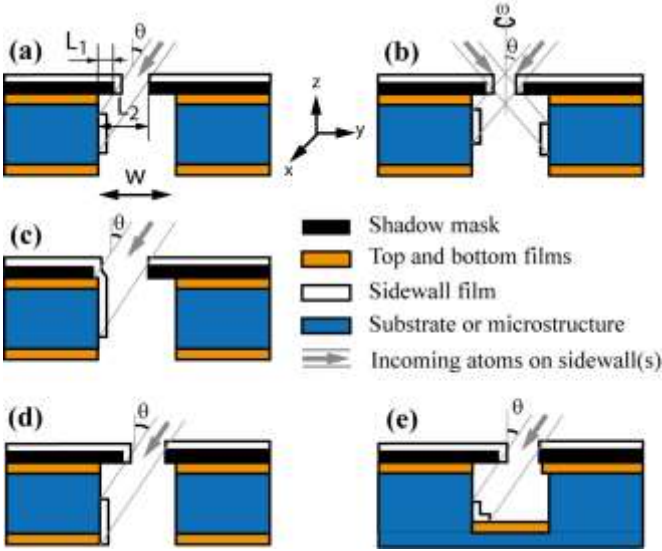


Figure 1. Principle of the patterning process. (a) Isolated sidewall film pattern, (b) Film patterns on both sidewalls ($\omega > 0$), (c) Sidewall film pattern connected to a top film, (d) Sidewall film pattern connected to a bottom film, (e) Sidewall film pattern connected to a film at the bottom of the aperture.

exposure, etching or deposition at oblique incidence can be used [4-10]. If the film is deposited by a conformal technique, patterning can be achieved by combining photoresist spray coating, the use of a standard photolithographic mask, tilted UV exposure and etching [4,5]. This process was recently improved by using immersion lithography with an absorbing ink to limit parasitic reflections [6]. Issues related to thickness non uniformity of resist spray coating might be overcome by using the resist coating process proposed in [11] which relies on the bending by stiction of photoresist cantilevers fabricated over the trench. Another way to perform film patterning on vertical sidewalls could be to pattern the conformal film by tilted reactive ion etching through an inorganic apertured membrane [7]. For directional film deposition techniques like evaporation, tilted deposition is a convenient method [7-9]. If electrodes are needed only on the top parts of the device and microstructure, a maskless process using shadowing effect by the adjacent structure might be sufficient [7]. Nevertheless, in the general case, a shadow mask is required. The shadow mask can be an apertured membrane fabricated and aligned on the device [8], or an external single level or multilevel silicon shadow mask mechanically aligned on the device wafer [9].

In this work, we investigate a version of the patterning technique based on tilted evaporation through a shadow mask that is greatly simplified thanks to the use of a dry photoresist film for the shadow mask. We initially proposed this process for the patterning of Au/Cr electrodes on the sidewalls of a piezoelectric semi-insulating GaAs 3 axis gyroscope microstructure, to allow vertical motion detection

[12]. In this paper we provide a detailed description and analysis of this deposition and patterning process notably in the case of wafer rotation during deposition. Principle and implementation are detailed in section 2. Then, in section 3, we provide a full modelling of the process to determine the shape, the thickness and the density distribution of the lateral electrode. It is compared in section 4 to experimental results in the case of Au/Cr patterns deposited on the sidewalls of deep trenches made by deep reactive etching in GaAs.

2. Principle and implementation of the patterning process

The principle of the investigated deposition and patterning process of a film on the sidewall of an aperture made in a wafer or a microstructure is depicted in figure 1 in various cases. It is based on the combination of tilt evaporation and shadow masking. The drawings are cross sections in the plane of incidence. The flow of atoms bounded by the shadow mask and arriving on the sidewall at the beginning of the deposition process is schematically drawn. There is a slight shadow mask aperture reduction by film deposition on the top and on the sidewall of the shadow mask. It leads to a thickness gradient at the top and bottom edges of the deposited pattern on the sidewall. This effect will be neglected in this paper because we will only consider the case where the film thickness is much lower than the mask aperture and trench height.

Figure 1(a) corresponds to the patterning of an isolated lateral electrode and a non rotating substrate. The pattern geometry is defined by the oblique incidence θ , the width W of the trench and the shadow mask overhangs (L_1 and $W - L_2$). Without rotation, the pattern thickness is expected to be dependent on its position on the wafer [13,14]. When the substrate is rotated like in figure 1(b), the pattern geometry on the opposite sidewall will be different if $L_1 \neq W - L_2$. This must be taken into account in the electrodes layout design. When the left overhang is zero or negative, the sidewall electrode can be connected to a top electrode (see figure 1(c)). Likewise, when θ is well chosen, according to the length $W - L_2$ of the right overhang, a connection can be achieved to an electrode at the rear surface of the wafer, like in figure 1(d), or to an electrode at the bottom of the trench, like in figure 1(e). For a through wafer opening, connection of a sidewall film to a film deposited at the rear surface can also be achieved by using configuration of figure 1(c) after flipping the wafer. Figure 1 shows that this patterning process is quite versatile but needs a careful electrode layout and shadow mask design notably when the substrate is rotated. A modelling of the dependence of pattern geometry on shadow mask parameters with and without rotation is given in section 3.

The practical implementation of the patterning process is

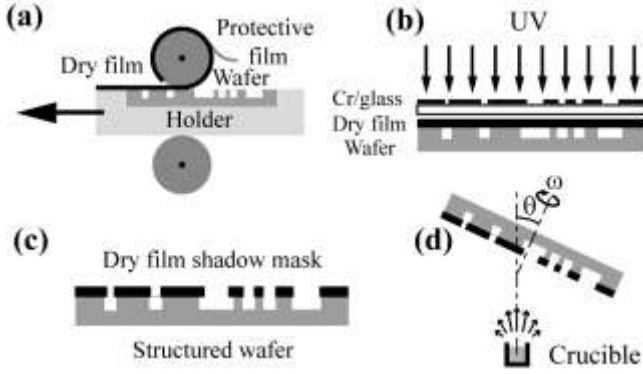


Figure 2. Flowchart of the patterning process.

shown in figure 2. Instead of using an external Si shadow mask or a membrane fabricated on the etched wafer as in previous works [9,10], we use a dry photoresist film laminated on the etched wafer (figure 2(a)) which is then patterned by UV photolithography with a standard aligner (figure 2(b)). This leads to an aligned shadow mask on the wafer after development (figure 2(c)). Then the wafer is introduced in an e-beam evaporation set-up allowing deposition under oblique incidence (figure 2(d)). Contrary to an external shadow mask mechanically aligned, the dry film shadow mask can only be used once but its optical alignment with an UV masker is more accurate and without the risk of damaging the microstructures. It is also easier to make than a direct fabrication of a membrane on the etched wafer. Indeed membrane fabrication requires the filling of apertures and a planarisation step before resist coating and photolithography [8,9]. Experimental details and results will be given in section 4.

3. Modelling of the patterning process

The aim of this section is to predict the shape and thickness distribution of the film deposited on the sidewall of a trench. It depends on the geometric parameters of the e-beam evaporator, notably the tilt angle, on the size and alignment of the aperture in the dry film shadow mask, and on the position of the trench on the wafer. We will first analyse the case of tilted deposition on the wafer surface, then we will consider the case of sidewall deposition without rotation of the wafer. Finally, we will study the impact of a rotation of the wafer.

3.1 Modelling of tilted deposition

The dependence on oblique incidence of incoming evaporated species of the deposition rate was modelled for the e-beam evaporation set-up used (PLASSYS Bestek 550S). The geometrical configuration during deposition at oblique incidence is schematically drawn in figure 3. In this set up, the tilt axis is not in the wafer plane: the center of rotation O of the wafer holder for deposition at oblique

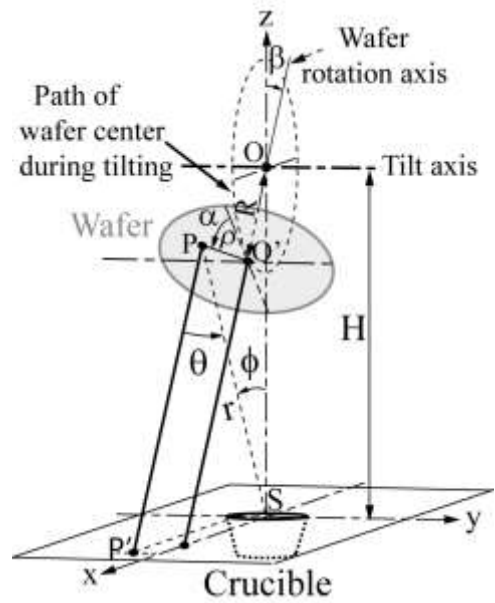


Figure 3. Geometry of film deposition at oblique incidence (Not to scale, H divided by a factor 4).

incidence is at a distance R to the wafer surface center O' . Consequently, during tilting, the wafer undergoes a non negligible translation in x direction and the true oblique incidence θ on the wafer surface is different from the tilt angle β even in the centre of the wafer. The minimum distance between the wafer surface centre and the crucible occurs at normal incidence and is equal to $H - R$. It is considered sufficiently large (650 mm) with respect to the crucible diameter (17 mm), the radius R (62.5 mm) and the wafer radius (50 mm) to allow the crucible to be approximated as a small area directed source for all points P on the wafer surface.

Let us consider a point P on the wafer top surface with polar coordinates ρ and α , at a distance r from the crucible, at an angle ϕ with respect to the crucible normal, and with oblique incidence θ (see figure 3). It can be shown that the deposited thickness t is given by [13-17].

$$t = \frac{1}{\mu} \frac{dm}{dA} = \frac{m}{\pi\mu} \left(\frac{n+1}{2} \right) \frac{\cos\theta \cos^n\phi}{r^2} \quad (1)$$

where m is the total mass of evaporated material, μ the film density, and n an exponent that depends on evaporation conditions. In the following we will consider $n = 1$. This is valid for low deposition rates and crucibles with low depth to diameter ratio [17].

Let P' be the intersection of the normal at point P and the crucible plane and S be the crucible centre (see figure 3). If \wedge denotes the vector product and (\cdot) the scalar product, θ can be expressed, after some trigonometric computations, as a function of the coordinates of point P , of the tilt angle β , and of the geometric parameters H and R :

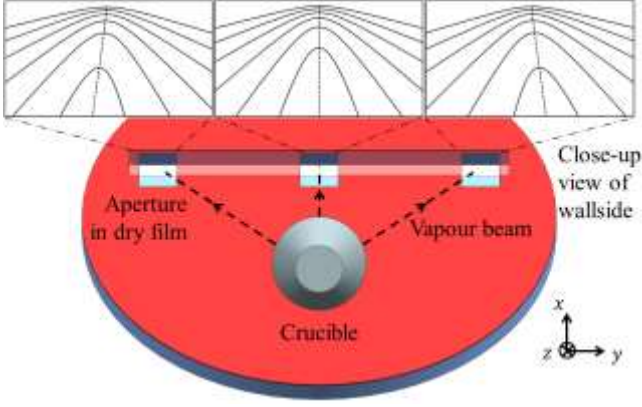


Figure 4. A wafer with an etched trench covered by dry film observed from behind the crucible (not to scale). For three apertures in the dry film, corresponding hyperbolas on the sidewall created by rotation of the wafer holder (see section 3.3) are plotted for β ranging from 10° (bottom line) to 60° (top line) with steps of 10° . Tops of the hyperbolas are connected by a dashed line to better show the asymmetry of pattern shape when the aperture is not in the (xOz) plane.

$$\tan \theta = \frac{\| \overline{PP'} \wedge \overline{PS} \|}{(PP' | \overline{PS})} \quad (2a)$$

$$= \frac{[(\rho \sin \alpha)^2 + (H \sin \beta + \rho \cos \alpha)^2]^{\frac{1}{2}}}{H \cos \beta - R} \quad (2b)$$

In the following, we will consider the point P to be on the sidewall of a straight trench partially covered with a dry film creating an overhang. To simplify the computations, we will assume that the direction of the trench is initially perpendicular to the plane (xOz) (see figure 3). A trench filling this condition is shown in figure 4. This means that, to apply the model without rotation described in the next section, the orientation of the wafer on the wafer holder must be carefully adjusted before deposition. In addition, we will consider that the mask aperture is centred with respect to (xOz) plane so the angle α is equal to zero. We will see later that this is not a large limitation of the model as long as ρ is low with respect to distance r , and angle β is sufficiently large.

3.2 Case of a non-rotating wafer

In the case of a non-rotating wafer the pattern thickness is expected to be quasi-uniform along the trench as its length is usually very low with respect to its distance to the crucible. Another film deposition after a 180° rotation of the wafer would be needed to pattern electrodes on the opposite sidewall. Likewise, other depositions after rotations of 90° and -90° would be required for the patterning of electrodes on the sidewalls of perpendicular trenches.

It is clear from figure 5 that the vertical location and size of the pattern depends on the overhang L_1 , on the opening L_2 –

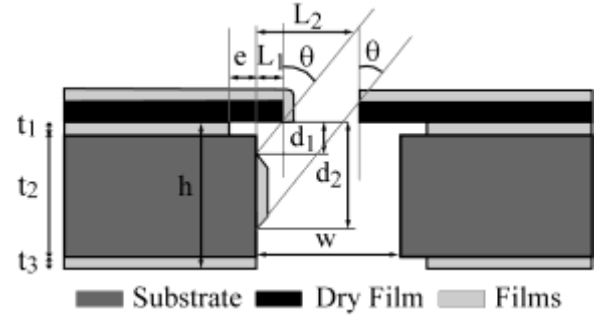


Figure 5. Pattern geometry defined by shadow masking with tilted deposition without wafer rotation

L_1 of the shadow mask and on incidence angle θ . It can be seen that the thickness of the shadow mask has no effect on the top border of the sidewall film pattern but it shifts upward its lower border: it reduces d_2 by an amount equal to the shadow mask thickness. Likewise, film deposition on the top of the dry film gradually shifts the lower border of the pattern and film deposition on the dry film edge gradually shifts the upper border of the pattern. To simplify the computations, we will consider, in the following and in the next section, that t_1 , t_3 and the thickness of the dry film are equal to zero and we will neglect the effect of film deposition on the top and edge of the shadow mask. Let W be the width of the trench. If the condition:

$$W \geq L_2 > L_1 \geq 0 \quad (3)$$

is filled, the depths d_1 and d_2 are simply related to L_1 and L_2 by:

$$\begin{cases} L_1 = d_1 \tan \theta \\ L_2 = d_2 \tan \theta \end{cases} \quad (4)$$

Consequently:

$$L_1/d_1 = L_2/d_2 \quad (5)$$

and:

$$\theta = \tan^{-1}(L_1/d_1) = \tan^{-1}(L_2/d_2) \quad (6)$$

To maximize the film deposition rate and density, the angle of incidence on the sidewall must be minimized and thus the value of θ ($0 \leq \theta < 90^\circ$) must be maximized. Consequently, according to equation (6), the values of L_1 and L_2 must be maximized while keeping true the conditions (1) and (5). The optimized solution is:

$$L_2 = W, L_1 = L_2 d_1/d_2, \theta = \tan^{-1}(W/d_2) \quad (7)$$

Using equation (2), it is possible to compute the associated angle β . Note that once β is set, the dimensions L_1 and L_2 must be adapted for trenches elsewhere on the wafer because θ depends on the coordinates (ρ, α) of the considered position on the wafer.

To get a connection with a top electrode with a recess e (see

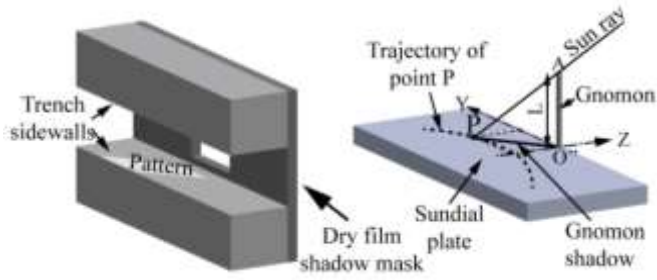


Figure 6. Analogy of shadow masking and operation of a sundial for an edge of the shadow mask aperture.

figure 5) we must have $L_1 \leq -e$. Let us emphasize that the film porosity will be different on the top part and on vertical sidewall if the incidence angle is different from 45° . A full connexion with a non-recessed bottom electrode on the rear surface can be achieved by using the conditions given by equation (7) and by setting $d_2 = h$, where h is the thickness of the wafer. If the rear electrode is recessed, the sample must be flipped during evaporation, and the condition given above for a connection to the top electrode must be used.

These different conditions might be difficult to fulfil for devices with a large range of trench widths and electrode geometries. So, devices with trenches having similar widths should be designed to apply this patterning technique. As this is also a requirement to limit aspect ratio dependent etching, in deep reactive ion etching processes, this is not so a critical issue.

3.3 Case of a rotating wafer

The case of patterning sidewall electrodes on straight trenches on a rotated wafer is much more complex but allows film deposition and patterning on every trench sidewall in a single run. As shown in figure 1(b), the pattern geometry will generally be different on the opposite side of the trench. Actually to get the same geometry, the overhang of the shadow mask must be the same on both sides of the trench, i.e. $L_1 = W - L_2$. When the substrate is rotated during deposition, the pattern geometry becomes variable along the trench length. This effect can be modelled by analogy with a sundial and by using gnomonics, the art of making and using sundials [18]. Indeed, we can consider each edge of the shadow mask rectangular aperture as a gnomon of a sundial, the crucible as the sun, the trench sidewall as the sundial plate with a horizontal position at equator and the pattern shape border as the path travelled by the gnomon shadow on the sundial plate (see figure 6). Four different gnomons, corresponding to the four edges of the rectangular aperture, have to be taken into account to determine the borders of the shape on the trench. The two gnomons of length $L = L_1$ delimit the top of the electrode while the two gnomons of length $L = L_2$ delimit the bottom of the electrode.

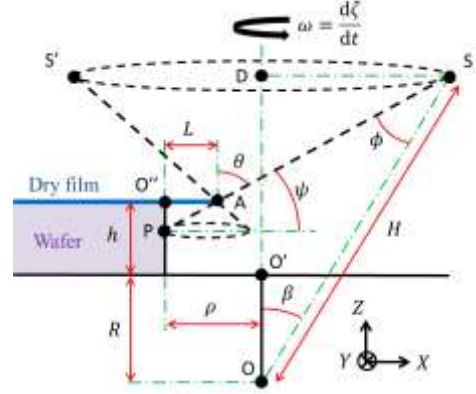


Figure 7. Half section of a trench of height h and its overhang of length L on a rotating wafer when $\zeta = 0^\circ$. S' is the image of S by a rotation of 180° , D is the centre of the circle passing by S and S' . A is the point at the end of the dry film. The trajectory of the point P on the sidewall is a conic. Note that a new reference (XYZ) different from (xyz) presented in figures 3 and 4 is used.

Equation 1 shows that the thickness, at any sample location, is the ratio of the deposited mass of the material and of its density. Both depend on the local angle of incidence of the vapour beam on the considered surface. We will first determine the pattern shape and thickness distribution on a trench sidewall from the deposited mass, then the density distribution in the pattern from the measured dependence of density with incidence angle, and finally the thickness distribution by taking into account the density distribution.

For the mathematical modelling, it is more convenient to consider the crucible rotating and the sample fixed as shown in figure 7. Each pattern border is then a conic corresponding to the intersection of the sidewall of the trench and the cone described by the point A as the apex (the end of the gnomon) and by the circle made by the crucible centre S around the rotation axis.

The initial orientation of the wafer at rotation angle $\zeta = 0^\circ$ is chosen such as the trench is perpendicular to the plane (xOz) . O'' is the point at the corner on the top of the trench. In the new frame of reference $(O''XYZ)$, we can express the coordinates of points A , S and D , where D is the centre of the circle made by S during rotation (see figure 7).

$$A: (X_A, Y_A, Z_A) = (L, 0, 0)$$

$$S: (X_S, Y_S, Z_S) = (H \sin \beta + \rho \cos \alpha, \rho \sin \alpha, H \cos \beta - R - h) \quad (8)$$

$$D: (X_D, Y_D, Z_D) = (\rho \cos \alpha, \rho \sin \alpha, H \cos \beta - R - h)$$

To predict the pattern shape on the sidewall, we will use a mathematical procedure valid in the general case but to simplify the mathematical expressions, we will establish the analytical formula only in the case $\alpha = 0^\circ$ represented in figure 4 for the central aperture. We will see later that this is an acceptable simplification of the general case. We thus rewrite the coordinates of points A , S and D in the case

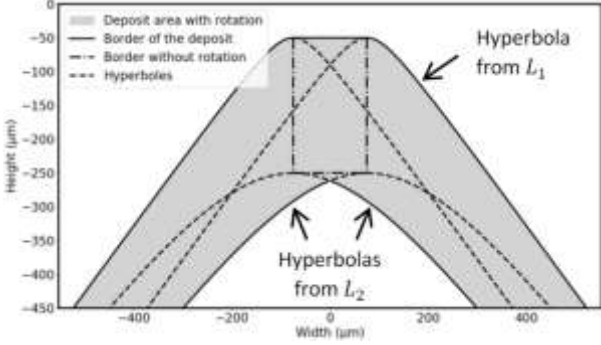


Figure 8. Shape of the lateral deposit with width aperture of $150 \mu\text{m}$ and parameters: $L_1 = 50 \mu\text{m}$, $L_2 = 250 \mu\text{m}$, $W = 300 \mu\text{m}$, $\rho = 0 \text{ mm}$, $\beta = 41.4^\circ$ and $h = 450 \mu\text{m}$.

where $\alpha = 0^\circ$:

$$A: (X_A, Y_A, Z_A) = (L, 0, 0) \quad (9a)$$

$$S: (X_S, Y_S, Z_S) = (H \sin \beta + \rho, 0, H \cos \beta - R - h) \quad (9b)$$

$$D: (X_D, Y_D, Z_D) = (\rho, 0, H \cos \beta - R - h) \quad (9c)$$

We express the equations of the lines (AS) and (AD).

$$(AS) \begin{cases} Y = 0 \\ Z_S(X - L) + (L - X_S)Z = 0 \Leftrightarrow X = L + \frac{X_S - L}{Z_S} Z \end{cases} \quad (10a)$$

$$(AD) \begin{cases} Y = 0 \\ Z_S(X - L) + (L - X_D)Z = 0 \Leftrightarrow X = L + \frac{X_D - L}{Z_S} Z \end{cases} \quad (10b)$$

At a given Z constant, the equation of the cone is the equation of the circle whose centre is on (AD) and intersecting (AS).

$$\left(X - L - \frac{X_D - L}{Z_S} Z \right)^2 + Y^2 = \frac{(X_S - X_D)^2}{Z_S^2} Z^2 \quad (11)$$

The conic described by the shadow of the gnomon is the intersection between the cone from equation (11) and the plane ($YO''Z$) $\Leftrightarrow X = 0$. By using equations (9a), (9b), (9c) and (11) we find the equation of the conic in the frame of reference ($O''XYZ$):

$$\frac{(\rho - L)^2 - H^2 \sin^2 \beta}{(H \cos \beta - R - h)^2} Z^2 + Y^2 + 2L \frac{\rho - L}{H \cos \beta - R - h} Z + L^2 = 0 \quad (12)$$

This equation has a physically valid solution, i.e. with negative Z , if one of the following conditions is true:

$$0 \leq L < \rho \quad (13)$$

$$|\sin \beta| > \frac{|\rho - L|}{h_0} \quad (14)$$

A negative value of L would correspond to the other side of the trench (not represented in figure 7 to simplify the drawing) with $L = L_2 - W$ for the top border of the pattern shape and $L = L_1 - W$ for the bottom border. If equation (14) is true, the border of the pattern shape on the sidewall is a hyperbola. This is the common case. If equation (13) is true, the pattern shape depends on another condition.

$$-\frac{|\rho - L|}{h_0} \leq \sin \beta \leq \frac{|\rho - L|}{h_0} \quad (15)$$

If equation (15) is a strict inequality, the pattern shape is an ellipse, whereas if it is an equality, the pattern shape is a parabola. Usually, the overhang length is much lower than the wafer radius ($L \ll \rho$). In that case, we can compute the maximum angle $\beta_{max} = \sin^{-1}(\rho/h_0)$ to get an ellipse. For $\rho = 50 \text{ mm}$ this would give $\beta_{max} = 4^\circ$. This case is not convenient in practise because for such a tilt, the film deposition rate and density on the sidewalls would be very low.

Figure 8 shows the computed pattern shape for a chosen set of deposition parameters close to the ones used in our experiments. When compared to the pattern shape without rotation (dot-dash line), its bottom is strongly deformed whereas its top is similar in the common width range. The presence of the hyperbolas in the rectangular area shows that the rotation also influences this zone by shading some parts.

The calculation above was made for a mask aperture centred in the trench like the one in the middle in figure 4. The effect of a lateral shift of the aperture is illustrated in the top of figure 4. It leads to an asymmetry of the hyperbolas that depends on the sign of coordinate $y = \rho \sin \alpha$ of the aperture. The deformation is visible, especially for low value of β , but it remains small when ρ is small with respect to the distance r between the crucible and the considered location P . Adding the fact that β is often higher than 20° , the simplifying assumption $\alpha = 0^\circ$ is generally a good approximation for the modelling of the pattern shape. In the case of non-rotating wafer (section 3.2), the amplitude of deformation is even lower because the surface of the sidewall exposed to vapour beam is smaller.

Beside a pattern shape distortion, the deposited film thickness and density are not uniform because the incidence angle and the deposited mass of metal vary with position. To compute the thickness distribution in the pattern shape, we use equation (1) but we replace $\cos \theta$ by $\cos \psi$ (see figure 7) because the deposition is done on the sidewall. We also simplify the equation by considering the approximation $\|\vec{SP}\| \approx \|\vec{SA}\|$. Indeed we have $\|\vec{SP}\|^2 = \|\vec{SA}\|^2 + \|\vec{AO''}\|^2 + \|\vec{O''P}\|^2$ with $\|\vec{SA}\|^2 > (H - R - h)^2$ while $\|\vec{AO''}\|^2 = L^2 \ll (H - R - h)^2$ and $\|\vec{O''P}\|$ is less than the length of the trench which is usually far less than $(H - R - h)^2$. So the deposited thickness on the sidewall is given by:

$$t = \frac{m \cos \psi \cos \phi}{\pi \mu \|\vec{SP}\|^2} \approx \frac{m \cos \psi \cos \phi}{\pi \mu \|\vec{SA}\|^2} \quad (16)$$

In equation (16), the density μ is dependent on the incidence angle ψ but we will first consider it constant along the trench. We express the coordinates of the points S , A and O in the frame of reference ($O''XYZ$) but we now take into

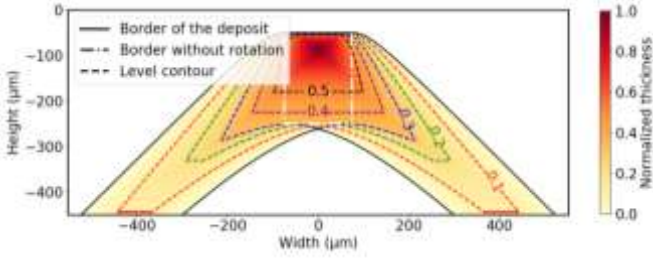


Figure 9. Film thickness normalized distribution in a trench sidewall pattern when the film density μ is considered constant. Same deposition parameters as for figure 8.

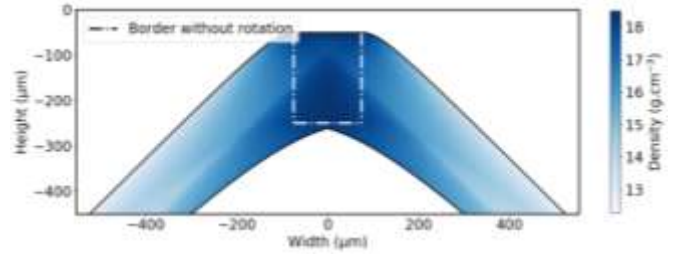


Figure 11. Estimation of one turn average density μ of a lateral deposit. Same deposition parameters as for figure 8.

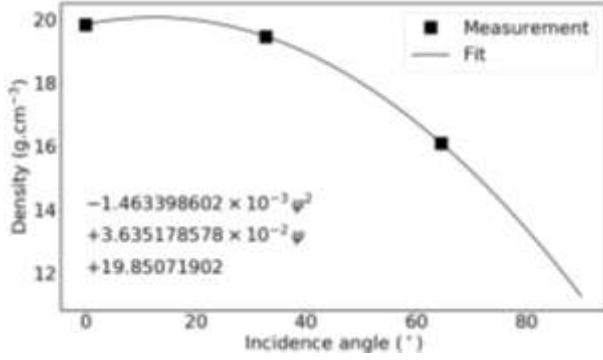


Figure 10. Measured film density as function of incidence angle.

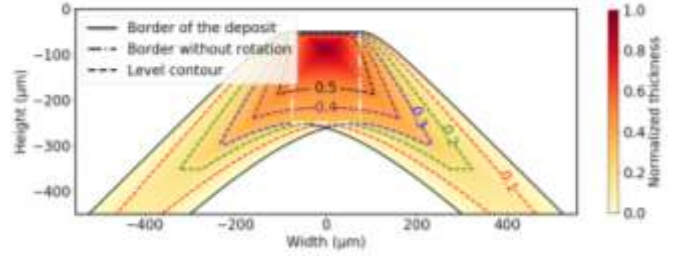


Figure 12. Film thickness normalized distribution in a trench sidewall pattern when the variation of the deposited film density μ with angle of incidence is taken into account. Same deposition parameters as for figure 8.

into account the rotation angle ζ of the wafer:

$$A: (L, 0, 0)$$

$$S: (H \sin \beta \cos \zeta + \rho, -H \sin \beta \sin \zeta, H \cos \beta - R - h) \quad (17)$$

$$O: (\rho, 0, -R - h)$$

We compute the distance $\|\overrightarrow{SA}\|^2$ as:

$$\|\overrightarrow{SA}\|^2 = H^2 + (R + h)^2 + (\rho - L)^2 + 2H(\rho - L) \sin \beta \cos \zeta - (R + h) \cos \beta \quad (18)$$

We get the values of $\cos \phi$ and $\cos \psi$.

$$\cos \phi = \frac{(\overrightarrow{SA}|\overrightarrow{SO})}{\|\overrightarrow{SA}\|\|\overrightarrow{SO}\|} = \frac{(\overrightarrow{SA}|\overrightarrow{SO})}{\|\overrightarrow{SA}\|H} = \frac{H - (R + h) \cos \beta + (\rho - L) \sin \beta \cos \zeta}{\|\overrightarrow{SA}\|} \quad (19)$$

$$\cos \psi = \frac{(\overrightarrow{AS}|(1,0,0))}{\|\overrightarrow{SA}\|} = \frac{H \sin \beta \cos \zeta + \rho - L}{\|\overrightarrow{SA}\|} \quad (20)$$

The insertion of equations (18), (19) and (20) into equation (16) allows the determination of the thickness variation $t(\zeta)$. To take into account the deposition at different values of ζ during rotation, we integrate $t(\zeta)$. For each point within the pattern shape (figure 8) and each angle ζ between $-\pi$ and π , we numerically compute the intersection point between the line (SP) and the plane $(XO''Y) \Leftrightarrow Z = 0$. If this point is inside the mask aperture, the vapour beam reaches the sidewall. So we compute the

associated thickness $t(\zeta)$ and use it for the integration, otherwise, we ignore it. In figure 9, the result of such integration is shown for a chosen set of parameters. It gives the thickness distribution in the pattern when the sample is rotated. As we considered a constant density μ , we normalized the thickness to its maximum value. Figure 9 shows that for the chosen deposition parameters, the film thickness decreases by more than 60 % in the targeted area and continues to decrease along the hyperbolas.

Actually the density μ is not constant in the deposited area. In order to evaluate the variation of the density as a function of the incidence angle, three deposits Au/Cr were done with $\beta = 0^\circ, 30^\circ$ and 60° on a plain wafer. The targeted thickness were 200 nm at 0.3 nm s^{-1} for the gold film and 20 nm at 0.1 nm s^{-1} for the chromium adhesion promoting sublayer. Thanks to a Sartorius microbalance having a $0.3 \mu\text{g}$ repeatability, the gold film density was measured by weighting 1 cm^2 coated Si dies at the centre of the wafer before and after selective Au layer etching in a $\text{KI}:\text{I}_2:\text{H}_2\text{O}$ bath. For the simulation, the Au film density was arbitrarily fitted by a 2nd degree polynomial to estimate its value between the measurement points (Figure 10).

By using this polynomial and equation (20), we can plot the map of a one turn average of the density μ in the deposited area (figure 11). It is quite constant in the targeted area and decreases along the hyperbolas arms. Then, by using equation (16), the normalized thickness distribution can be evaluated by taking into account the variation of film density μ . The result is shown in figure 12. When compared

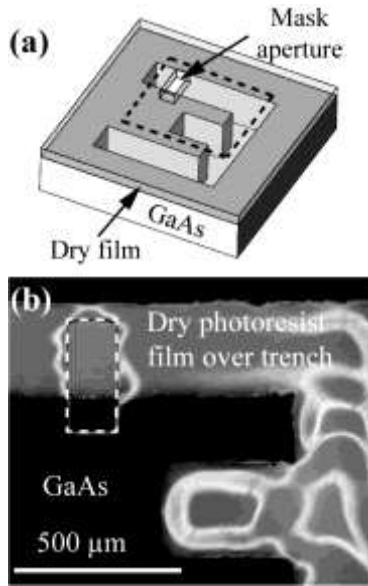


Figure 13. (a) Schematic 3D drawing of deep trenches in a GaAs wafer coated with a dry film masking layer. A small rectangular aperture is designed to make a connection between the top surface and a lateral side. (b) Top view image of the sample area delineated by black dashed lines in the 3D drawing. The mask aperture is shown by white dashed lines.

with figure 9 where μ is supposed constant, the thickness in the hyperbolas arms is slightly higher, as expected from figure 11. For example, it increases the size in the arms of the 0.1 normalized level contours. Nevertheless, it finally does not change the general predicted pattern shape of the deposited electrode on the sidewall.

4. Implementation and results of the patterning process

The proposed process was applied to the patterning of lateral electrodes on structures with trenches around fabricated by bulk micromachining of 450 μm thick semi-insulating GaAs wafers. This substrate material was chosen because the patterning process was initially intended as a fabrication step of a 3 axis GaAs piezoelectric gyroscope [12]. Deep reactive ion etching (DRIE) in BCl_3/Cl_2 plasma was used as the etching technique. Various geometries were investigated with narrow or wide lateral electrodes connected to top electrodes. In all cases, rotation of the wafer holder was activated during deposition. After fabrication, the samples were inspected with a Keyence VHX-5000 digital optical microscope.

4.1 Shadow mask fabrication

The dry film used for shadow mask fabrication is a MX5015 negative photoresist from Dupont company having a thickness of 15 μm . Its top face is protected by a polyester film and its bottom face by a polyethylene (PET) film. Dry

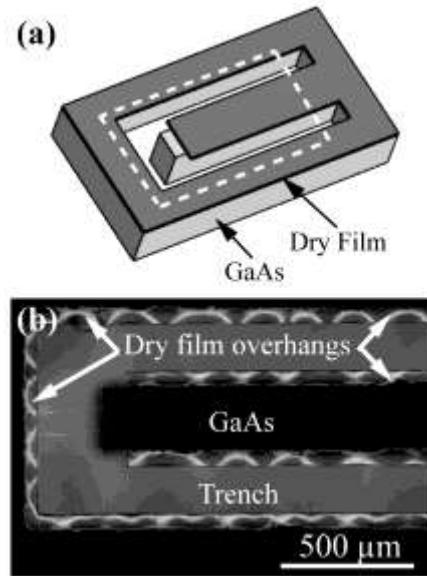


Figure 14. (a) Schematic 3D drawing of a bulk micromachined GaAs clamped-free beam after dry film lamination and photolithography. The dry film mask is not covering the beam end to allow a connection between the top and the lateral electrodes. (b) Top view image of the sample area delineated by white dashed lines in the 3D drawing.

film lamination with bottom PET film removal was performed on 100 mm in diameter semi-insulating GaAs wafers with a laminator (Model 4200 from Think and Tinker company). After some preliminary tests, the heating roll temperature was adjusted to 100 $^{\circ}\text{C}$ and the lamination roll speed to 5 rpm. The roll pressure was set to its minimum value in order to reduce the risk of breaking the device. This is also favourable to a lower deformation of the dry film. By using a recessed wafer holder during dry film lamination (see figure 2(a)), this lamination could be made on wafers with deep trenches or through-wafer etched areas without breaking. After lamination the coated wafer was transferred to an EVG 620 mask aligner. The dry film was exposed to UV with a total dose of 50 mJ cm^{-2} then baked 5 min at 100 $^{\circ}\text{C}$ on a hot plate. The protective polyester film was then peeled off and the dry film was developed in a MRD4000 bath for 1 min 30 s.

These conditions lead to resist patterns with quasi vertical sidewalls and a minimum pattern size larger than 5 μm . This shadow mask is thus only suitable for relatively large apertures. Dry films with a thickness down to 5 μm are available so shadow masks compatible with smaller trenches and patterns could be done. However, thinner is the dry film, larger might be its deformation induced by mechanical stress generated by its processing or by the evaporated film stress.

Figures 13 and 14 show optical microscope pictures of narrow and wide apertures made in a dry film over 300 μm wide through wafer trenches. White lines can be observed in the dry films over the trenches. They are due to reflectance

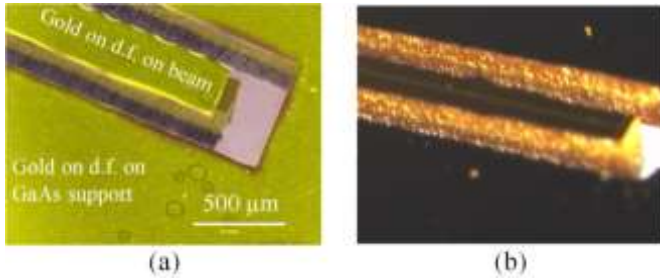


Figure 15. Optical microscopy images with enhanced colors of parts of a clamped-free beams with lateral electrodes (a) before and (b) after lift-off of the dry film (noted d.f.). A connection from sidewall to top electrode is visible at the end of the beam.

variations by ripples of the dry film. These ripples are more or less sinusoidal in the dry film overhangs along the trench borders (see figure 14). They can be attributed to dry film buckling induced by compressive stress generated during dry film processing. Phase shifting interferometry measurements showed that these ripples have an amplitude of a few hundreds of nm. They are expected to degrade the pattern shape on the sidewall by a similar amount. Over large trenches, an additional downward deflection of the dry film was also observed. For example, a 1 μm general bow was measured over a 300 μm wide trench. Nevertheless, the dry film adhesion remained good enough to make apertures over 300 μm wide trenches without observing dry film delamination.

4.2 Film patterning on vertical sidewalls of trenches

Au/Cr film deposition was performed in a Plassys Bestek 550S e-beam evaporation set-up which allows a tilt angle in the 0 to 90° range. High purity Cr and Au pellets were successively evaporated after outgassing from 15 cm^3 alumina crucibles. The background pressure was 1.3×10^{-8} mbar before evaporation and 1.3×10^{-7} mbar during evaporation. This evaporation set-up is equipped with a quartz microbalance that allows a monitoring of the deposition rate that would occur at normal incidence. It was calibrated from thickness measurements of films deposited on flat Si wafers without tilt.

The etched GaAs dies covered with dry films have an area of about $1 \times 1 \text{ cm}^2$. They were placed at the centre of the wafer holder. The film depositions were performed with a tilt angle $\beta = 46^\circ$ and a wafer rotation speed of 5 rpm. The selected deposition conditions provide, at normal incidence, a 10 nm thick chromium adhesion promoting layer with an evaporation rate of 0.1 nm s^{-1} , and a 400 nm thick gold film with a deposition rate of 0.3 nm s^{-1} .

Figure 15 shows lateral electrodes deposited all around a free-clamped beam on half of its thickness. The bottom border of the lateral electrode does not appear sharp even at this scale because GaAs DRIE, contrary to Si DRIE, produces trenches with a high sidewalls surface roughness.

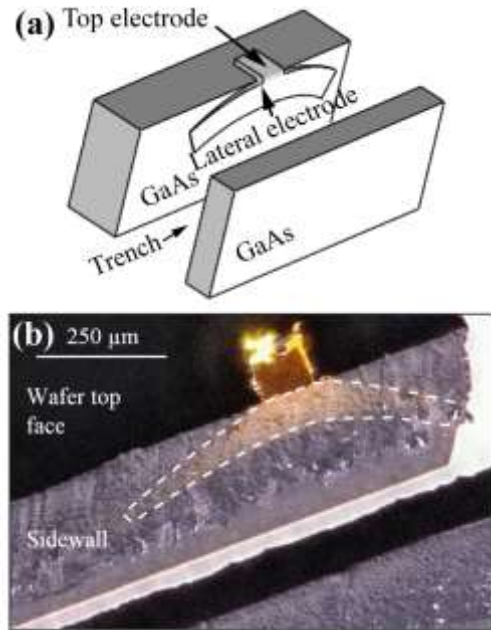


Figure 16. (a) Schematic 3D drawing of the expected shapes of the top and lateral electrodes on a deep trench when a rectangular mask opening like in figure 13 is used and when the wafer is rotated during deposition. (b) Tilted view image of a trench after patterning Au/Cr electrodes through a 150 μm wide shadow mask aperture with $L_1 = 0$ and $L_2 = 220 \mu\text{m}$. The borders of the electrode on the trench sidewall are approximately drawn in dashed lines to show the hyperbolic-like shape of the deposited film.

The lateral electrode border (not visible in figure 15) presents a hyperbolic deformation but it remains small with respect to the length of the electrode. Nevertheless, this result demonstrates that this patterning process is suitable for the design of long lateral electrodes only connected to the top electrode on both sides of trenches.

As shown above in figure 12, for rotated substrates and narrow apertures, the model detailed in section 3.3 predicts a decrease of the deposited film thickness and density on a trench sidewall outside the shadow mask opening. On a rough surface and for a non-conformal deposition technique like evaporation, this density reduction is larger because of local shadowing effects by asperities. A direct comparison of the model with experiments is quite difficult because there is not a common technique able to measure thickness distribution of a metallic film on a rough trench sidewall. Nevertheless, we can clearly observe in figure 16 that the optical contrast between the Au film and the GaAs surface is a decreasing function of the distance to the shadow mask opening. Optical calculation showed that both the normal incidence optical reflectance of a gold film and its contrast on a smooth GaAs surface become high only for wavelengths in the visible-NIR range above about $0.55 \mu\text{m}$. In this wavelength range, the reflectance contrast decreases rapidly when the gold film thickness is lower than about 50 nm. From the optical microscopy image of figure 16, we could then very roughly estimate that the film thickness is lower

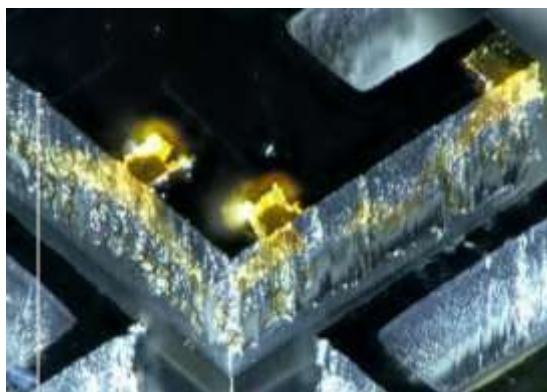


Figure 17. Three sets of top and lateral Au/Cr electrodes obtained with a dry film shadow mask patterned with narrow rectangular apertures.

than 50 nm beyond a lateral distance equal to $\approx 75 \mu\text{m}$ and a vertical distance equal to $\approx 150 \mu\text{m}$ from the shadow mask edge. Actually, the light absorption of an Au film is decreasing with film density so this distance can be significantly underestimated.

A major limitation of the investigated process for patterning lateral electrodes is illustrated in figure 17. When two narrow electrodes are located on the same sidewall, the hyperbolic deformation of the patterned electrodes induced by wafer rotation during deposition can create an electric short circuit, even with a quite large space between them. This must be considered during the mask layout design or a slight metal film etch has to be performed after deposition. Another way to overcome this limitation could be to change the shape of the mask aperture or of the sidewall.

5. Conclusion

A simple process applicable at the wafer scale and allowing the deposition and alignment of patterned electrodes on the vertical sidewalls of microstructures is demonstrated and analyzed in details. It is based on tilted evaporation through a dry film photoresist shadow mask having a specific design. The sidewall patterns can be connected or not to bottom or top electrodes by a suitable alignment of the shadow mask edges. The proposed process can be applied to any evaporated films that must be patterned on the vertical walls of trenches with a width approximately equal to 1/3 to 1/2 of the dry film thickness. A first specific limitation of the process is the stress-induced distortion of the dry film shadow mask edges during dry film processing. This issue might be increased or decreased by the deposited film residual stress. Rotation of the wafer during the evaporation allows the deposition and patterning of films on every sidewalls simultaneously but it leads to a hyperbolic deformation of the laterak electrode borders. This must be considered in the mask design or corrected after deposition. A mathematical model predicting the shape and the thickness

of a lateral electrode with or without rotation has been developed. It could be applied or adapted to all patterning processes based on tilt deposition, tilt etching or tilt lithography.

Acknowledgements

This work was performed in the frame of two PhD theses grants supported by DGA and ONERA. Film deposition and measurements were performed in the micro/nano fabrication platform of C2N supported by the Renatech French national network. The authors wish to thank Marie-Paule Pante and David Bouville for their assistance in clean rooms for film deposition and photolithography respectively.

References

- [1] Westerik P J, Vijselaar W J C, Berenschot J W, Tas N R, Huskens J and Gardeniers J G E 2017 Sidewall patterning—a new wafer-scale method for accurate patterning of vertical silicon structures *J. Micromech. Microeng.* **28** 015008 doi: [10.1088/1361-6439/aa9c20](https://doi.org/10.1088/1361-6439/aa9c20)
- [2] Vijselaar W, Westerik P, Veerbeek J, Tiggelaar R M, Berenschot E, Tas N R, Gardeniers H and Huskens J 2018 Spatial decoupling of light absorption and catalytic activity of Ni–Mo-loaded high-aspect-ratio silicon microwire photocathodes *Nat. Energy* **3** 185–92 doi: [10.1038/s41560-017-0068-x](https://doi.org/10.1038/s41560-017-0068-x)
- [3] Xu J, Wu D, Ip J Y, Midorikawa K and Sugioka K 2015 Vertical sidewall electrodes monolithically integrated into 3D glass microfluidic chips using water-assisted femtosecond-laser fabrication for in situ control of electrotaxis *RSC Adv.* **5** 24072–80 doi: [10.1039/C5RA00256G](https://doi.org/10.1039/C5RA00256G)
- [4] Morii H, Oohira F, Suzuki T, Terao K, Sasaki M, Ochi T, Yuzuriha A and Wani K 2011 Proposal of High-Density Packaging Construction and Conductive Pattern Forming Method on Vertical Wall Using Spray Coating Technology *IEEJ Transactions on Sensors and Micromachines* **131** 40–4 doi: [10.1541/ieejsmas.131.40](https://doi.org/10.1541/ieejsmas.131.40)
- [5] Yamaguchi T, Shibata M, Kumagai S and Sasaki M 2015 Thermocouples fabricated on trench sidewall in microfluidic channel bonded with film cover *Jpn. J. Appl. Phys.* **54** 030219 doi: [10.7567/JJAP.54.030219](https://doi.org/10.7567/JJAP.54.030219)
- [6] Kumagai S, Kubo H and Sasaki M 2017 Light-absorbent liquid immersion angled exposure for patterning 3D samples with vertical sidewalls *J. Micromech. Microeng.* **27** 025016 doi: [10.1088/1361-6439/aa5429](https://doi.org/10.1088/1361-6439/aa5429)
- [7] Borden P G and Walsh R V 1982 Silicon solar cell with a novel low-resistance emitter structure *Appl. Phys. Lett.* **41** 649–51 doi: [10.1063/1.93636](https://doi.org/10.1063/1.93636)
- [8] Burckel D B, Finnegan P S, Henry M D, Resnick P J and Jarecki R L 2016 Oblique patterned etching of vertical silicon sidewalls *Appl. Phys. Lett.* **108** 142103 doi: [10.1063/1.4945681](https://doi.org/10.1063/1.4945681)
- [9] Burckel D B, Wendt J R, Eyck G A T, Ginn J C, Ellis A R, Brener I and Sinclair M B 2010 Micrometer-Scale Cubic Unit Cell 3D Metamaterial Layers *Adv. Mater.* **22** 5053–7 doi: [10.1002/adma.201002429](https://doi.org/10.1002/adma.201002429)
- [10] Morishita S, Kim J H, Marty F, Li Y, Walton A J and Mita Y 2009 A three-dimensional silicon shadowmask for patterning on

- trenches with vertical walls *TRANSDUCERS 2009 - 2009 International Solid-State Sensors, Actuators and Microsystems Conference* pp 1608–11 doi: [10.1109/SENSOR.2009.5285767](https://doi.org/10.1109/SENSOR.2009.5285767)
- [11] Wasa K, Saito S, Sahara F and Sasaki M 2018 Patterning vertical sidewall using standard aligner *2018 IEEE Micro Electro Mechanical Systems (MEMS)* pp 475–8 doi: [10.1109/MEMSYS.2018.8346592](https://doi.org/10.1109/MEMSYS.2018.8346592)
- [12] Piot A, Bourgeteau B, Le Traon O, Roland I, Isac N, Levy R, Lavenus P, Guérard J and Bosseboeuf A 2015 Electromechanical and process design of a 3 axis piezoelectric MEMS gyro in GaAs *2015 DGON Inertial Sensors and Systems Symposium (ISS)* pp 1–16 doi: [10.1109/InertialSensors.2015.7314260j](https://doi.org/10.1109/InertialSensors.2015.7314260j)
- [13] Pulker H K 1999 *Coatings on Glass* 2nd edn (New York: Elsevier)
- vapor deposition chambers for lens coating *J. Vac. Sci. Technol. A* **10** 98–104 doi: [10.1116/1.578073](https://doi.org/10.1116/1.578073)
- [15] Holland L and Steckelmacher W 1952 The distribution of thin films condensed on surfaces by the vacuum evaporation method *Vacuum* **2** 346–64 doi: [10.1016/0042-207X\(52\)93784-6](https://doi.org/10.1016/0042-207X(52)93784-6)
- [16] Wang J, Shao J, Yi K and Fan Z 2005 Layer uniformity of glancing angle deposition *Vacuum* **78** 107–11 doi: [10.3390/coatings8090325](https://doi.org/10.3390/coatings8090325)
- [17] Wang B, Fu X, Song S, Chu H O, Gibson D, Li C, Shi Y and Wu Z 2018 Simulation and Optimization of Film Thickness Uniformity in Physical Vapor Deposition *Coatings* **8** 325 doi: [10.3390/coatings8090325](https://doi.org/10.3390/coatings8090325)
- [18] Vial A 2007 Lignes de déclinaison d'un cadran solaire plan d'orientation quelconque *Bulletin de l'Union des Professeurs de Physique et de Chimie* **101** 981–98Z

- [14] Bosch S 1992 Computer-aided procedure for optimization of layer thickness uniformity in thermal evaporation physical